

Electronic Supplementary Material

Vanadium oxide cathode pillared by Al^{3+} and H_2O for high-performance aqueous zinc-ion batteries

Li Xu^{1,2}, Xincheng Wang¹, Shoubo Li¹, Wenyu Zhang¹, Yuchen Wang¹,
and Yae Qi (✉)¹

1 College of Chemistry and Chemical Engineering, Hexi University; Key Laboratory of Hexi Corridor Resources Utilization of Gansu, Zhangye 734000, China

2 State Key Laboratory of Molecular Engineering of Polymers, Fudan University, Shanghai 200433, China

E-mail: qiyazhu@163.com

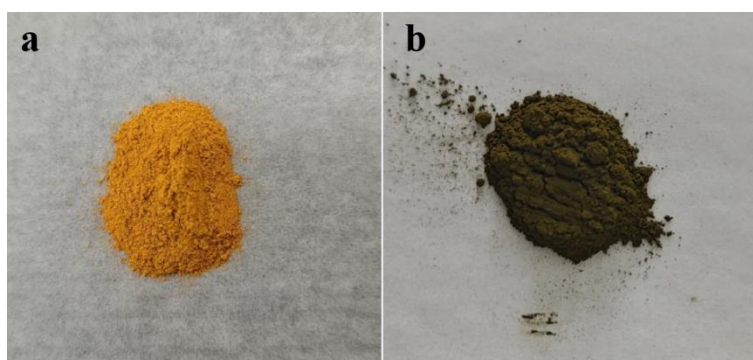


Fig. S1 Optical photographs: (a) $\text{c-V}_2\text{O}_5$; (b) AlVO.

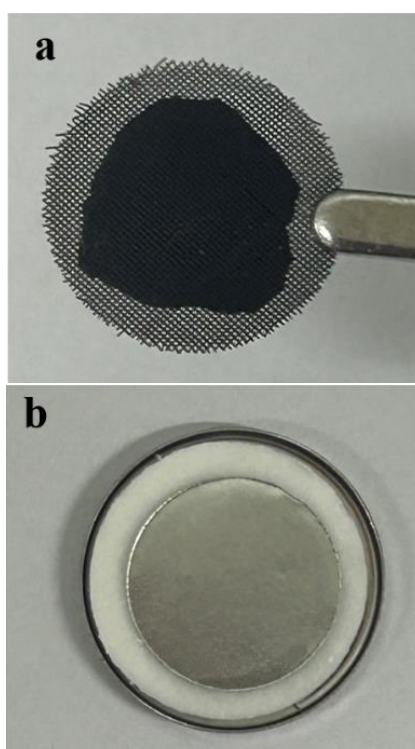


Fig. S2 Optical photographs: (a) cathode; (b) Waterman glass fiber separator and Zn metal anode.

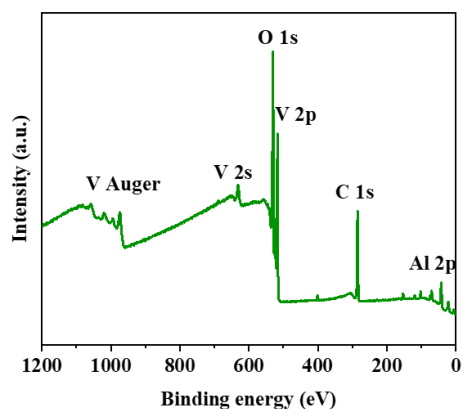


Fig. S3 Full XPS survey spectrum of PPy- V_2O_5 .

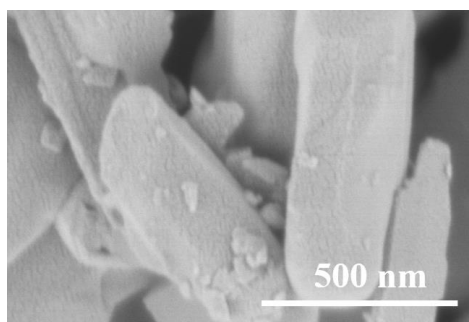


Fig. S4 SEM image of $c-V_2O_5$.

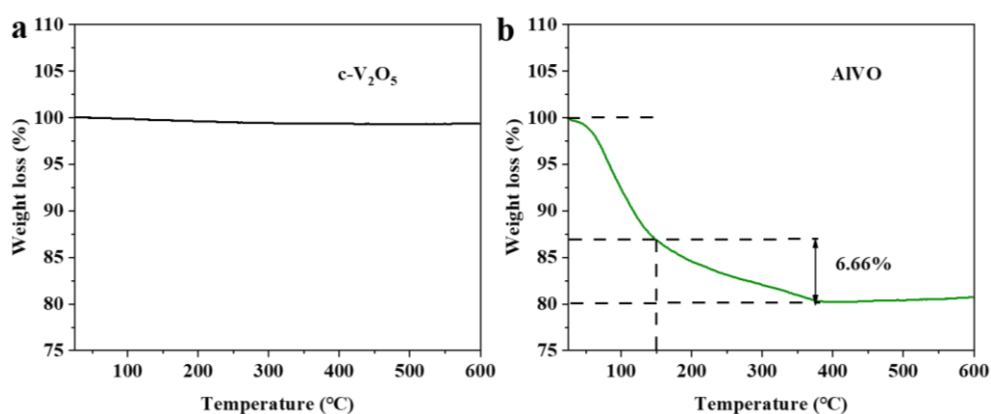


Fig. S5 TG curves of (a) $c-V_2O_5$ and (b) AlVO.

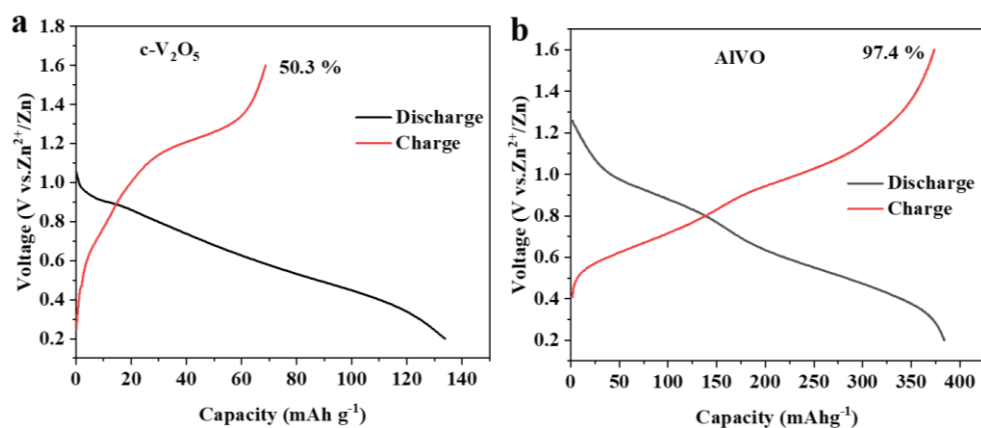


Fig. S6 The first discharge/charge profiles of two batteries at $0.5 \text{ A} \cdot \text{g}^{-1}$: (a) Zn// $c-V_2O_5$; (b) Zn//AlVO.

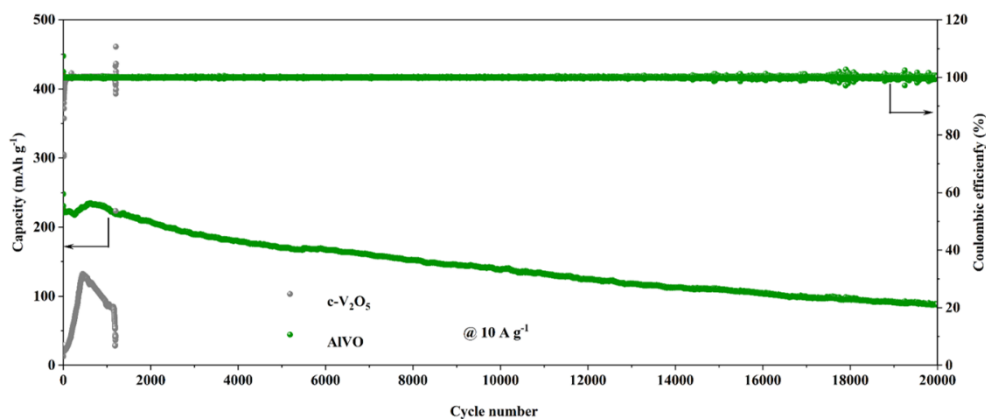


Fig. S7 Cycle performance of AIVO and $c\text{-V}_2\text{O}_5$ cathodes $10 \text{ A}\cdot\text{g}^{-1}$.

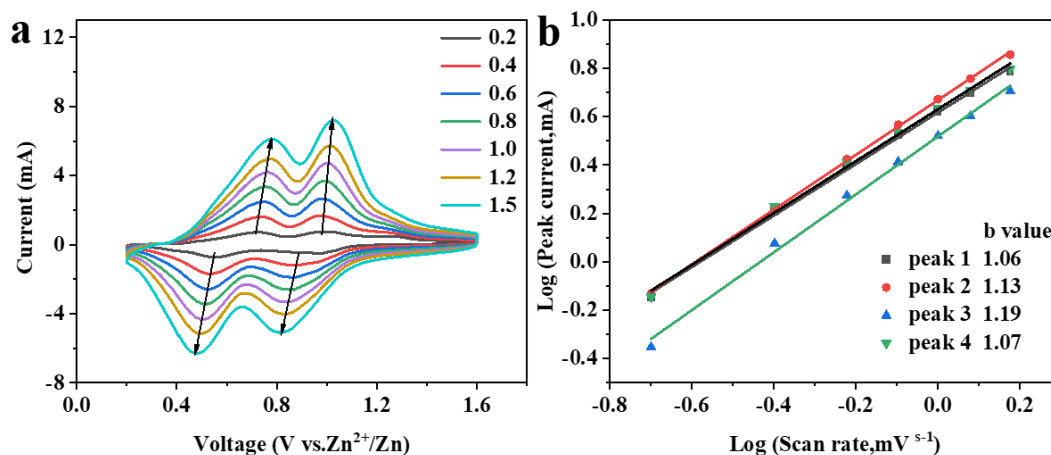


Fig. S8 (a) CV curves at different scan rates for the Zn//AIVO battery. (b) Relationships between the peak current and the scan rate.

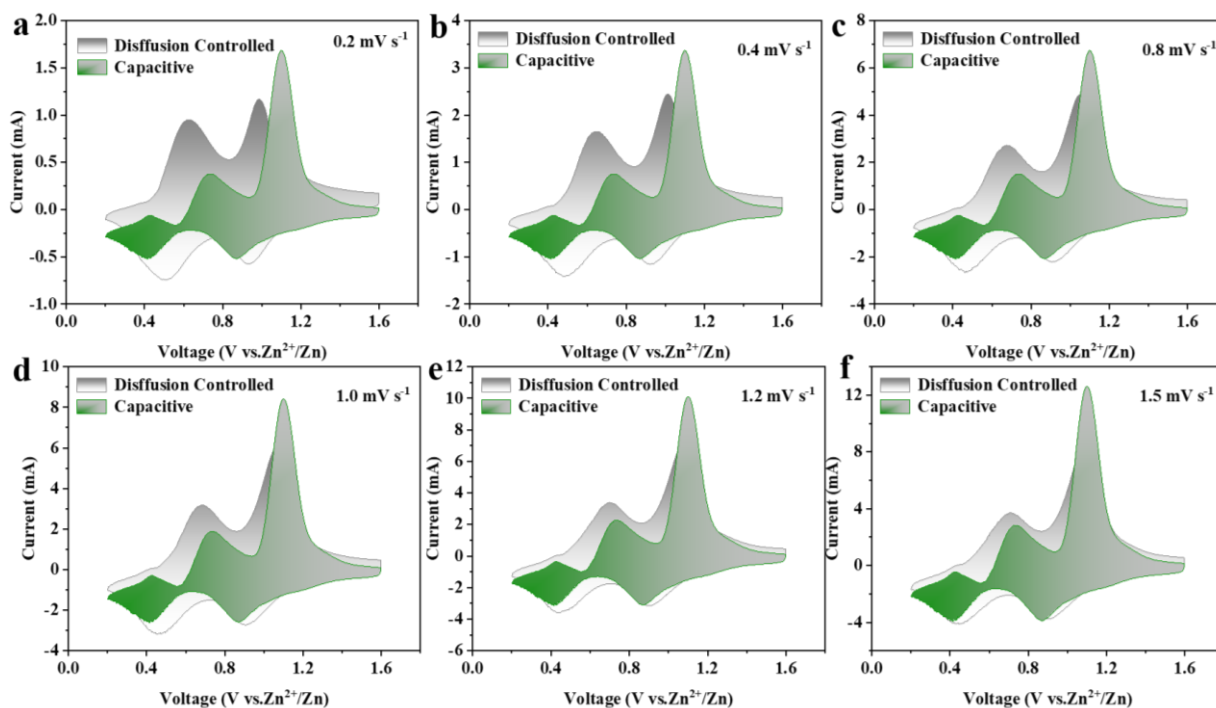


Fig. S9 Capacitance-controlled (green) and diffusion-controlled (gray) behaviors of the Zn//AIVO battery at (a) $0.2 \text{ mV}\cdot\text{s}^{-1}$, (b) $0.4 \text{ mV}\cdot\text{s}^{-1}$, (c) $0.8 \text{ mV}\cdot\text{s}^{-1}$, (d) $1.0 \text{ mV}\cdot\text{s}^{-1}$, (e) $1.2 \text{ mV}\cdot\text{s}^{-1}$, and (f) $1.5 \text{ mV}\cdot\text{s}^{-1}$.

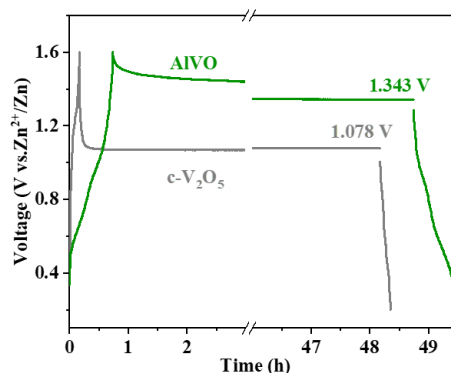


Fig. S10 Self-discharge performance of AlVO and $c\text{-V}_2\text{O}_5$ cathodes.

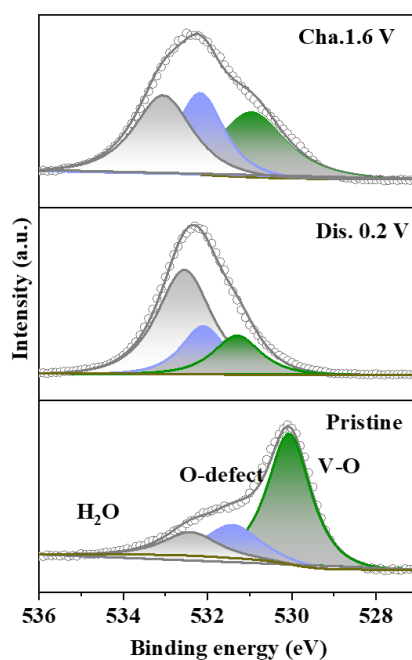


Fig. S11 *Ex-situ* high-resolution XPS spectra of O 2p at fully discharge/charge state in the first cycle at $0.5 \text{ A} \cdot \text{g}^{-1}$.

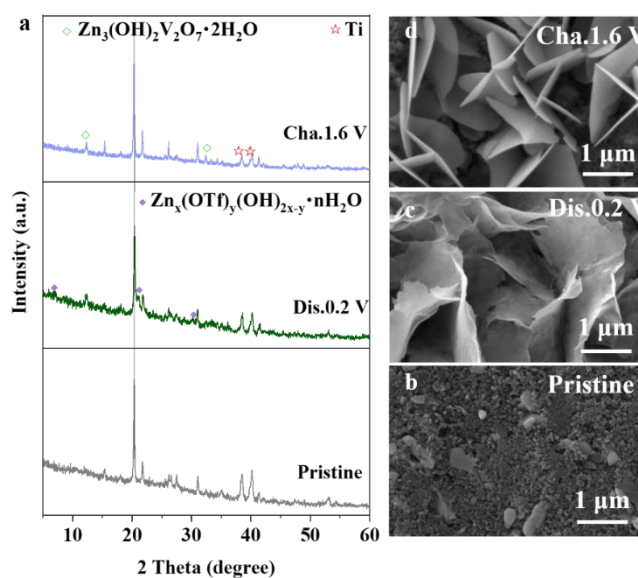


Fig. S12 (a) *Ex-situ* XRD patterns of the $c\text{-V}_2\text{O}_5$ cathode at different discharge/charge stages in the first cycle at $0.5 \text{ A} \cdot \text{g}^{-1}$. *Ex-situ* SEM images of the $c\text{-V}_2\text{O}_5$ cathodes: **(b)** pristine, **(c)** the 1st discharge to 0.2 V, and **(d)** the 1st charge to 1.6 V.

Table S1 Comparison of cycle performance of vanadium-based cathodes for AZBs

Cathode	Electrolyte	$C/(\text{mAh}\cdot\text{g}^{-1})$ (at $i/(\text{A}\cdot\text{g}^{-1})$)	Cycle performance (N ($i/(\text{A}\cdot\text{g}^{-1})$))	$C_f/(\text{mAh}\cdot\text{g}^{-1})$	Ref.
$\text{Sn}_{1.5}\text{V}_2\text{O}_7(\text{OH})_2\cdot 3.3\text{H}_2\text{O}$	–	300 at (0.1)	500 (10)	125	[S1]
MnVO	$3 \text{ mol}\cdot\text{L}^{-1} \text{ Zn}(\text{CF}_3\text{SO}_3)_2$	415 (0.05)	2000 (4)	264	[S2]
PEDOT- $\text{NH}_4\text{V}_3\text{O}_8$	$3 \text{ mol}\cdot\text{L}^{-1} \text{ Zn}(\text{CF}_3\text{SO}_3)_2$	356.8 (0.05)	5000 (10)	160.6	[S3]
VCN	–	256 (1)	1000 (5)	106	[S4]
NaVPO ₄ F	$15 \text{ mol}\cdot\text{L}^{-1} \text{ NaClO}_4 +$ $1 \text{ mol}\cdot\text{L}^{-1} \text{ Zn}(\text{CF}_3\text{SO}_3)_2$	87.4 (0.1)	4000 (1)	66.7	[S5]
$\text{Mg}_x\text{V}_2\text{O}_5\cdot n\text{H}_2\text{O}$	$1 \text{ mol}\cdot\text{L}^{-1} \text{ ZnSO}_4 +$ $1 \text{ mol}\cdot\text{L}^{-1} \text{ MgSO}_4$	374 (0.1)	200 (1)	180	[S6]
V_2O_5	30 m ZnCl_2	341 (0.05)	1000 (1)	138	[S7]
FeVO ₄	–	250 (0.1)	2500 (5)	70	[S8]
V_2O_5	$21 \text{ mol}\cdot\text{kg}^{-1} \text{ LiTFSI} +$ $1 \text{ mol}\cdot\text{kg}^{-1} \text{ Zn}(\text{CF}_3\text{SO}_3)_2$	238 (0.05)	2000 (2)	110	[S9]
$\text{K}_2\text{V}_8\text{O}_{21}$	–	230 (0.5)	300 (6)	128	[S10]
$\text{Mn}_{0.15}\text{V}_2\text{O}_5\cdot n\text{H}_2\text{O}$	$1 \text{ mol}\cdot\text{L}^{-1} \text{ Zn}(\text{ClO}_4)_2/\text{PC}$	367 (0.1)	8000 (10)	153	[S11]
AIVO	$3 \text{ mol}\cdot\text{kg}^{-1} \text{ Zn}(\text{CF}_3\text{SO}_3)_2$	390.7 (0.5)	10000 (10) 20000 (10)	138.2 89	This work

Notes: C , capacity; i , current density; N , cycle number; C_f , final capacity.

References

- [S1] Xu W, Sun C, Wang N, et al. Sn stabilized pyrovanadate structure rearrangement for zinc ion battery. *Nano Energy*, 2021, 81: 105584
- [S2] Liu C, Neale Z, Zheng J, et al. Expanded hydrated vanadate for high-performance aqueous zinc-ion batteries. *Energy & Environmental Science*, 2019, 12(7): 2273
- [S3] Bin D, Huo W, Yuan Y, et al. Organic–inorganic-induced polymer intercalation into layered composites for aqueous zinc-ion battery. *Chem*, 2020, 6(4): 968–984
- [S4] Chen Z, Hu J, Liu S, et al. Dual defects boosting zinc ion storage of hierarchical vanadium oxide fibers. *Chemical Engineering Journal*, 2021, 404: 126536
- [S5] Bin D, Wang Y, Tamirat A G, et al. Stable high-voltage aqueous zinc battery based on carbon-coated NaVPO₄F cathode. *ACS Sustainable Chemistry & Engineering*, 2021, 9(8): 3223–3231
- [S6] Zhang Y M, Li H N, Huang S Z, et al. Rechargeable aqueous zinc-ion batteries in MgSO₄/ZnSO₄ hybrid electrolytes. *Nano-Micro Letters*, 2020, 12: 60
- [S7] Tang X Y, Wang P, Bai M, et al. Unveiling the reversibility and stability origin of the aqueous V₂O₅–Zn batteries with a ZnCl₂ “water-in-salt” electrolyte. *Advanced Science*, 2021, 8(23): 2102053
- [S8] Luo Y, Wei L, Geng H, et al. Amorphous bimetallic oxides Fe–V–O with tunable compositions toward rechargeable Zn-ion batteries with excellent low-temperature performance. *ACS Applied Materials & Interfaces*, 2020, 12(10): 11753–11760
- [S9] Hu P, Yan M Y, Zhu T, et al. Zn/V₂O₅ aqueous hybrid-ion battery with high voltage platform and long cycle life. *ACS Applied Materials & Interfaces*, 2017, 9(49): 42717–42722
- [S10] Tang B, Fang G, Zhou J, et al. Potassium vanadates with stable structure and fast ion diffusion channel as cathode for rechargeable aqueous zinc-ion batteries. *Nano Energy*, 2018, 51: 579–587
- [S11] Geng H, Cheng M, Wang B, et al. Electronic structure regulation of layered vanadium oxide via interlayer

doping strategy toward superior high-rate and low-temperature zinc-ion batteries. *Advanced Functional Materials*, 2020, 30: 1907684